Proceedings of the Project Review, Geo-Mathematical Imaging Group (Purdue University, West Lafayette IN), Vol. 1 (2008) pp. 121-128.

GAUSSIAN BEAM IMAGING FOR CONVERTED AND SURFACE REFLECTED WAVES

ROBERT L. NOWACK*

Abstract. An overview of Gaussian beam imaging is given for converted and surface reflected seismic waves. The earthquake seismology community now regularly uses seismic waves from distant sources to illuminate structures beneath seismic arrays in so-called passive imaging experiments. Similarly, reservoir structures can be imaged with seismic waves incident from below using sources in boreholes. Gaussian beams are applied for passive imaging based on an over-complete frame-based Gaussian beam representation of the seismic wavefield. Paraxial Gaussian beams are then utilized for the propagation of the seismic waves back into the medium. The approach provides stable imaging of seismic data in smoothly varying background media where caustics and triplicated arrivals can exist. Gaussian beam imaging is found to be very flexible with respect to different experimental geometries and can be configured to allow for different types of converted or reflected waves. A synthetic example is first given for a collisional zone structure with an incident P-wave from below where several different scattered wave types are used to image the structure. Seismic data from the 1993 Cascadia experiment are then used to image the subduction zone beneath the Pacific Northwest in Oregon. The results from Gaussian beam imaging are found to compare favorably with imaging results obtained using ray/Born inversion.

1. Introduction. An overview of Gaussian beam migration for the imaging of converted and surface reflected seismic waves is given with application to passive imaging experiments (Nowack et al., 2006; Nowack et al., 2007a, b). A similar approach has been applied to common-shot data by Nowack et al. (2003). Scattered S-waves from incident P-waves have typically been used for passive imaging beneath seismic arrays, where radial receiver functions, with the source function removed, are constructed by deconvolving the radial component data with the vertical P-wave component (Vinnik, 1977; Langston, 1977, 1979; Owens et al. 1984). To image all components of the seismic data, auto- and cross-correlation techniques have been applied (Sheng, et al., 2001, 2003; Schuster et al., 2003, ; Yu et al., 2003; Schuster, 2008 and Dasgupta and Nowack, 2006), as well as multi-channel deconvolution (Bostock, 2004). For exploration geometries in reservoir structures, ghost reflections from the free surface can be used for imaging with sources in boreholes (Schuster et al., 2004; Schuster, 2008). Also, daylight interferometic methods can be applied for random source signals (Schuster et al., 2004; Schuster, 2008; Rickett and Claerbout, 1999)

For the imaging of receiver function data from distant sources, basic stacking techniques were initially applied (Dueker and Sheehan, 1997; Zhu, 2000). Seismic migration techniques were then applied for P to S conversions from seismic waves recorded by passive arrays (Bostock and Rondenay, 1999; Ryberg and Weber, 2000; Sheehan et al., 2000; Poppeliers and Pavlis, 2002 and Pavlis, 2003). Using a ray/Born imaging approach, Bostock et al. (2001) extended this to surface reflected phases, and Shragge et al. (2001) and Rondenay et al. (2001) applied this to seismic data from the 1993 Cascadia experiment

Gaussian beam migration uses an over-complete frame of smoothly localized Gasussian windows to represent the seismic data. Paraxial Gaussian beams are then used to propagate the data back into the medium. Since for Gaussian beam migration the source and back-propagated wavefield are decomposed into Gaussian beams, the imaging condition then uses individual Gaussian beams and allows for caustics, as well as triplicated seismic wavefields, in the background medium. In contrast, Kirchhoff migration or ray/Born inversions require the first arrivals or most energetic arrivals at the scatterer and this results in an incomplete imaging condition unless further analysis is performed. This is an advantage of Gaussian beam migration over other high-frequency migration approaches.

The Gaussian beam approach for passive imaging is first illustrated using synthetic seismic data for a collisional zone model similar to that used by Schragge et al. (2001). The approach is then applied to image seismic data from the 1993 Cascadia experiment and compared with the ray/Born inversion of Rondenay et al. (2001). The Gaussian beam inversion was found to compare favorably with the ray/Born approach and provide a somewhat cleaner image of the subduction zone.

*Dept. of Earth and Atmos. Sci., Purdue University, West Lafayette, IN 47907, USA (nowack@purdue.edu).

2. Overview of Gaussian Beam Imaging for Waves Incident from Below Structures. In a heterogeneous elastic medium, the Green's function, representing a propagating wave from an initial position $\underline{x}^g$ to a final position $\underline{x}'$, can be expanded as a sum of Gaussian beams (Popov, 1982; Cerveny et al., 1982; Nowack and Aki, 1984; Cerveny, 1985a,b; Cerveny, 2000; Nowack, 2003)

$$g_{ij}(\underline{x}', \underline{x}^g; \omega) = \int d\underline{\gamma}\, \Psi(\underline{\gamma}, \omega) u_{ij}^{\rm gb}(\underline{x}', \underline{x}^g, \underline{\gamma}, \omega) \tag{2.1}$$

where $u_{ij}^{\rm gb}$ are the individual Gaussian beams (GB), $\Psi(\underline{\gamma}, \omega)$ are weighting functions, $\underline{\gamma}$ specifies the initial direction of the central-ray of each beam ("ray-coordinates", for example, a ray with angle θ in 2-D), and ω is the angular frequency. Eqn. (2.1) can be used to describe either the P- or S-wave components of the Green's function in the far-field.

Each individual Gaussian beam can be written as

$$u_{ij}^{\rm gb}(\underline{x}', \underline{x}^g; \omega) = U_{ij}^{\rm gb}(\underline{x}', \underline{x}^g, \underline{\gamma}) {\rm e}^{{\rm i}\omega T(\underline{x}', \underline{x}^g, \underline{\gamma})} \tag{2.2}$$

where $U_{ij}^{\rm gb}(\underline{x}', \underline{x}^g, \underline{\gamma})$ includes the beam's amplitude, geometric spreading, any reflection/transmission coefficients, ray-dependent radiation patterns of the source, and polarization vector at positions along the beam's central ray.

For a beam solution, the phase term $T(\underline{x}', \underline{x}^g, \underline{\gamma})$, expanded to second-order away from the central ray, is real along the central ray and complex at positions off the central ray. The curvature matrix (used to describe the phase away from the central ray) is complex and positive-definite; and its real-part represents the curvature of the wave-front while the imaginary-part tapers the amplitude away from the central ray, thus forming a beam. By applying a paraxial or second-order approximation of the phase function away from the central ray, no two-point ray tracing is required for positions off the central ray. For the amplitude term, the geometric spreading is also complex, but it remains non-singular along the entire beam even at caustics.

The beam parameters are chosen at one point along the central ray and the dynamic ray equations are then used to compute values of the complex curvature matrix at other points along the ray (Cerveny, 2000). The beam parameters are commonly specified at either the initial or end point of the beam, although they can be specified at the scattering point as well.

As an example, in eqn. (2.3) below we show the formula of imaging using GB for the case of scattered SV-wavefield resulting from an incident P-wave. Formulas for other types of scattered waves have similar forms. For simplicity, we assume a 2-D geometry in a Poisson solid of constant density. Then the scattered wavefield can be expressed in terms of the perturbed shear modulus, $\delta\mu$, since for a Poisson solid, $V_p^2 = 3V_s^2$ (Aki and Richards, 1980; Nowack et al., 2006; Nowack et al., 2007a).

Under the Born approximation, the imaging condition is met by applying the adjoint of the linearized operator representing scattering and expanding the scattered SV-waves into Gaussian beams (Nowack et al., 2006)

$$I(\underline{x}') \sim \sum_L \int d\omega/(2\pi) C_1(\omega) \overline{S}(\omega) \bar{u}_i^0(\underline{x}', p_1^E, \omega) \int \frac{dp_1^g}{dp_3^g} \overline{\Psi}(p_1^g, \omega) \bar{u}_{i1}^{\rm gbSV}(\underline{x}', x^L, p_1^g, \omega) D(x^L, p_1^g, p_1^s, \omega) \tag{2.3}$$

where $I(\underline{x}')$ is the image in terms of perturbed shear modulus of the background medium. The summation is over the discretely sampled beam centers at a spacing of ΔL , where $x^L = L\Delta L$. In addition, $C_1(\omega) = (\omega/V_p)^2 \frac{\Delta L}{\sqrt{2\pi}\sigma}$ is a coefficient, where σ is the initial beam width at the receivers, being specified at a reference low-frequency.

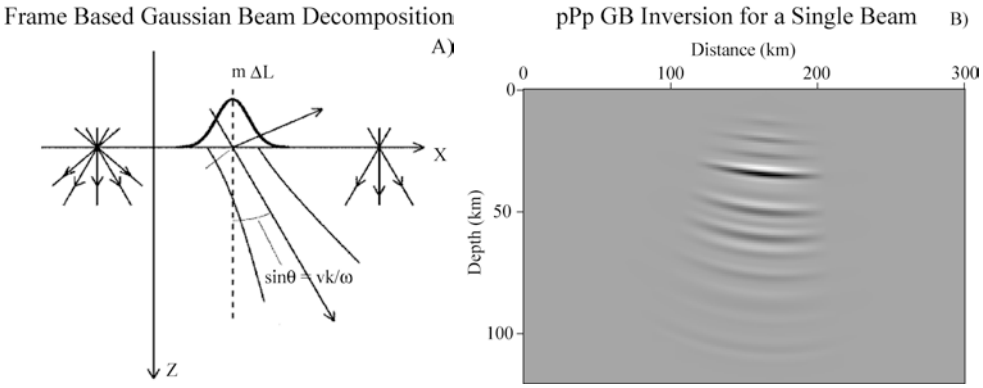

FIG. 1. *A) Frame-based Gaussian Beam decomposition. Initial wavefields are decomposed into Gaussian windowed beam components that are then launched at different angles into the medium. B) This shows an example of the back-propagation of a single Gaussian beam for a synthetic model given by Nowack et al. (2006).*

The integration over frequency ω results from the specific imaging condition adopted here. In the integrand, $\bar{u}_i^0(\underline{x}', p_1^E, \omega)$ is the complex conjugate of the incident P-wave at the scatterer locations $\underline{x}'$, where p_1^E is the horizontal component of the slowness vector of the incident P-wave, and $\bar{S}(\omega)$ is the source-time function where over-bars signify complex conjugates. p_1^g represents the horizontal component of the slowness vector along the seismic array (specified at the beam centers), and $\bar{u}_{i1}^{\mathrm{gbSV}}$ is the complex conjugate of the individual GB-component for the scattered SV-wave.

Finally, $\bar{\Psi}(p_1^g, \omega)$ is the complex conjugate of the weighting function in Eqn. (2.1), indexed in 2-D by the horizontal component of the slowness at the geophones, p_1^g. In the end, a summation is performed on the subscripts i, where i=3 if the incident wavefield is a near-vertical P-wave.

Also, in eqn (2.3),

$$D(x^L, p_1^g, p_1^E, \omega) = \int \mathrm{dx}^g \delta u_1(x^g, p_1^E, \omega) \mathrm{e}^{-(x^g - x^L)^2/2\sigma^2} \mathrm{e}^{\mathrm{i}\omega p_1^g (x^g - x^L)} \tag{2.4}$$

represents local slant-stacks of the horizontal-component of data (denoted by the subscript 1). Eqn (2.4) shows that the stacks are comprised of Gaussian-windowed data, $\delta u_1(x^g, p_1^E, \omega)$, where x^g is the horizontal-coordinate along the surface. In addition, p_1^E and p_1^g are the horizontal component of the slowness vector for the incident wave and for the GB, respectively (the latter is being back-propagated from surface at positions x^L). p_1^g is related to the take-off angle (θ, also the angle along which slant-stacks are taken) at the seismic array by $p_1^g = \frac{\sin\theta}{V_S}$. The terms that downward propagate the windowed and slant-stacked data into the subsurface are simply the paraxial Gaussian beams, $\bar{u}_{i1}^{\mathrm{gbSV}}(\underline{x}', x^L, p_1^g, \omega)$, for the case of scattered SV-wave observed at the receivers.

Figure 1A shows an example of seismic data being decomposed into initial beams as a function of position and angle and then propagated back into the medium. Figure 1B shows a synthetic example from Nowack et al. (2007a) of a single beam back-propagated into the medium.

3. Applications of Gaussian beam Migration to Passive Imaging. To illustrate the Gaussian beam approach for passively recorded seismic data, a synthetic example from Nowack et al. (2006) is given. The velocity model is shown in Figure 2 and is based on an idealized collisional zone model from Shragge et al. (2001). Vertical (Z comp) and radial (X comp) ray/Born synthetics have been generated and are shown in Figure 3, where the scattering is incorporated using point scatterers within a background two layer model similar to that used by Shragge et al. (2001) for their test migrations. More complete finite difference simulations have been performed by Nowack et al. (2007a), and similar inversion results were found for the Gaussian beam imaging. The source is a plane P-wave incident from below at a 20 degree angle from the vertical with a Gaussian source

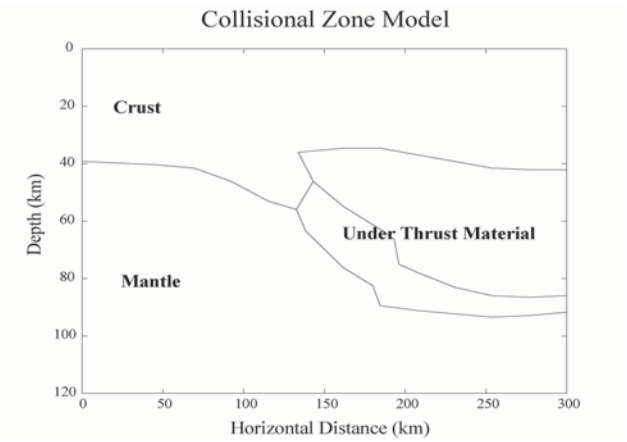

FIG. 2. *A collisional zone model used to test the Gaussian beam migration.*

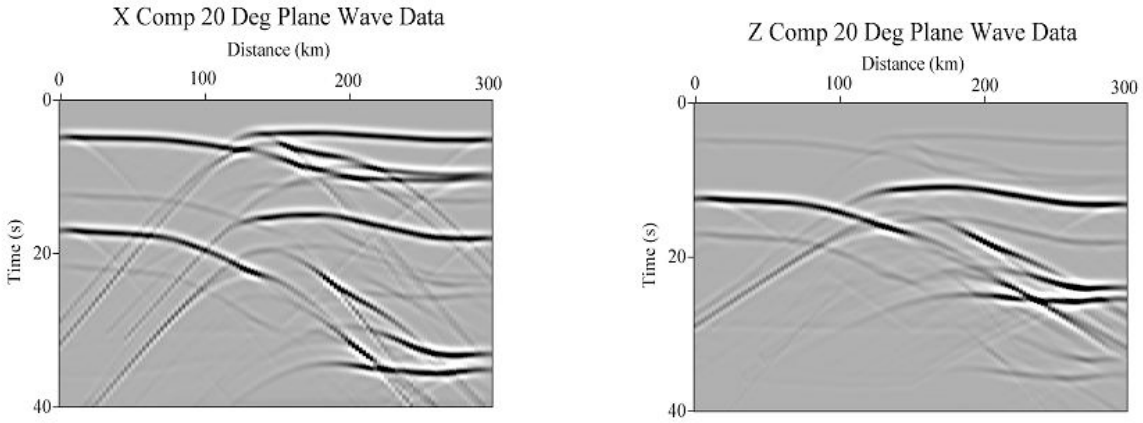

FIG. 3. *Ray/Born synthetics for the subduction zone model in Figure 2. The source P-wave is incident at 20 degrees from the vertical. The scattering is incorporated using point scatterers imbedded in a two-layer velocity structure. The modeled phases include the direct ps, and the surface reflected pPs, pSp, pSs and pPp phases. The seismograms have been shifted to correct for the incident angle. The direct P phase would arrive at time zero but has been muted out.*

pulse with a width of about 1 second. The seismograms in Figure 3 have been shifted using the incident angle and are displayed in a similar form as shown by Shragge et al. (2001). The modeled phases include the direct ps scattered phase on the X component and the surface reflected pPp, pPs, pSp and pSs phases. Note that for simplicity the initial P has been left off of the designations for the surface reflected phases. Thus the pPp indicates the wave that travels to the free surface as a P-wave, reflects at the free surface as a P and gets scattered back as a P. In Figure 3, the direct P arrival will arrive at zero time, but has been muted out.

In Figure 4, Gaussian beam migration has been applied to different phase types in Figure 3. For these examples an initial beamwidth of 30 km was used for a reference frequency of .1 Hz and a high frequency of 2 Hz. However, a range of values of initial beamwidths could be used following the relationships given by Hill (1990, 2001) and Hale (1992), as well as by general frame inequalities. In Figure 4A, the surface reflected pPp phase on the vertical component has been imaged and the subduction zone and Moho can be seen. The small artifacts are from other phases included in the synthetic data not imaged by this particular imaging condition. Figure 4B shows the image of

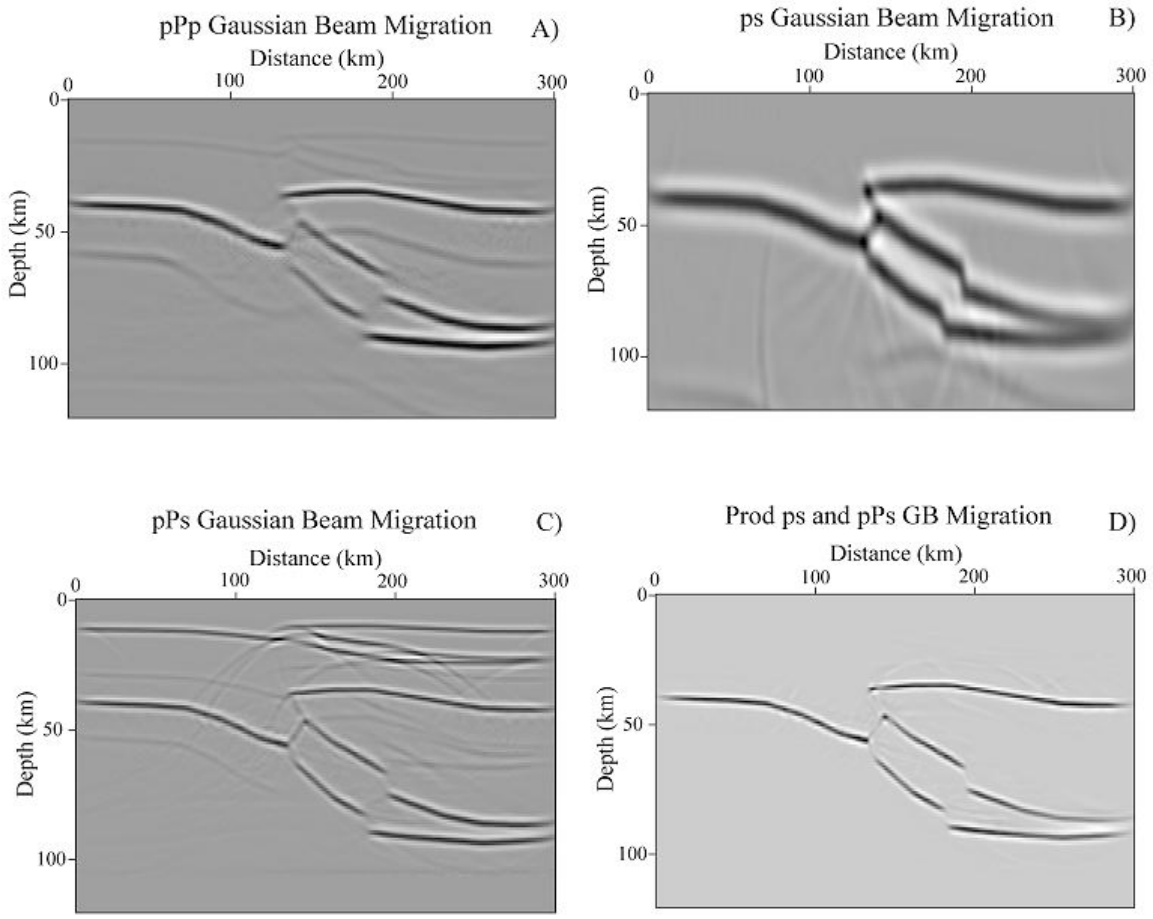

FIG. 4. *Gaussian beam migration of synthetic receiver functions in Figure 3. A) This shows the Gaussian beam migration of the surface reflected pPp phase on the Z comp. B) This shows the GB migration of the ps directed P-to-S scattered phase on the X comp. C) This shows the GB migration of surface reflected pPs phase on the X comp. Note the better depth resolution compared to the migration of the ps phase. D) This shows the product of the ps and pPs Gaussian beam migrations.*

the directly scattered ps phase on the radial component and is also well imaged. The pPs surface reflected phase is migrated in Figure 4C and in this case the non-imaged ps phase is still visible at the shallower depths. The pPs image in Figure 4C can be seen to be less stretched vertically than the image of the ps phase in Figure 4B and therefore provides better vertical resolution. In order to reduce the artifacts in the individual images in Figure 4, the images have been multiplicatively combined and the result is shown in Figure 4D. However, a more comprehensive procedure based on combining the images by a coherence weighted stack was developed by Sheng et al. (2003).

Figure 5 shows a comparison of imaging seismic data from a distant earthquake source from the 1993 Cascadia experiment. Seismic event 6 from Rondenay et al. (2001) is used for the comparison. Applying the ray/Born imaging approach of Bostock et al. (2001), Rondenay et al. (2001) imaged different scattered phases, and Fig. 5B shows their imaging results for the pPs phase. The pPs phase was found to provide some of the best imaging results for this experiment. For Gaussian beam imaging, the radial components of the data were first correlated with the vertical components to approximately remove the effects of the source time function. The data were then interpolated to a uniform 4 km spacing over the 200 km aperture of the linear array. The pPs phase was imaged using

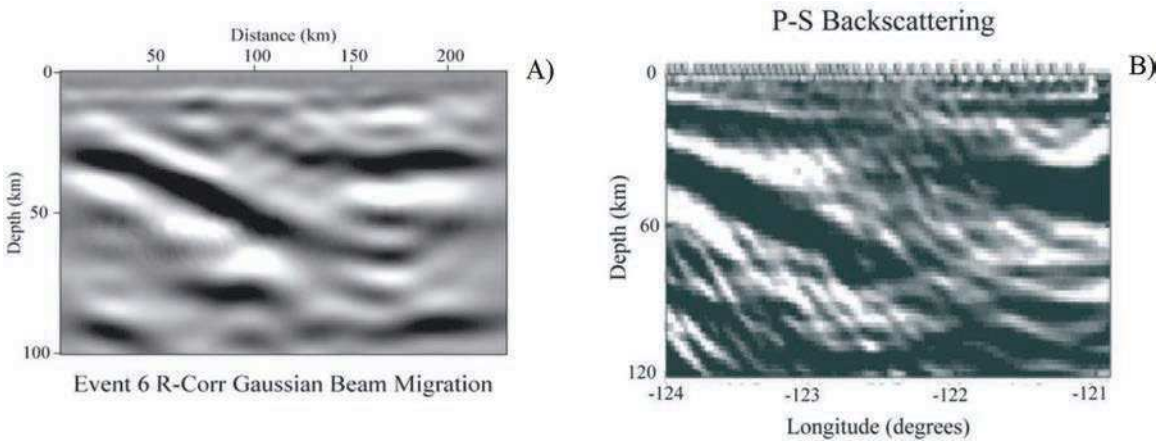

FIG. 5. *Comparison of the imaging results from the Gaussian beam migration approach and the Ray-Born approach. A) Gaussian beam imaging results from one event from the 1993 Cascadia experiment. B) Ray/Born imaging results of Rondenay et al. (2001) for same event from the Cascadia experiment.*

Gaussian beams, and the results are shown in Fig. 5A. The Gaussian beam results are somewhat smoother than the ray/Born results from both the trace interpolation and the smoothing from the Gaussian beam imaging. However, recent results from the Hi-CLIMB experiment in Tibet compared Gaussian beam imaging using a uniform station spacing from trace interpolation and by directly using an irregular station spacing in the Gaussian beam imaging and similar results were found (Nowack et al., 2007b). The comparisons in Figure 5 show that the results from Gaussian beam imaging compare favorably with the results from ray/Born inversion of Rondenay et al. (2001) and provide somewhat smoother images.

4. Conclusions. In this overview, Gaussian beam imaging has been described for converted and surface reflected waves with application to passively recorded seismic events. For exploration applications, the approach is also applicable to incident waves from below reservoir structures. Gaussian beam migration is based on an over-complete frame-based representation of the seismic wavefield, and uses paraxial Gaussian beams for the back-propagation of the seismic waves. This provides stable imaging of seismic data in smoothly varying background media where caustics and triplicated arrivals can exist. The Gaussian beam imaging method was first illustrated using synthetic data computed for a collisional zone model, and the results showed that Gaussian beam migration can image structures using different scattered wave types (Nowack et al., 2006). The Gaussian beam imaging method was then applied to observed seismic data from the 1993 Cascadia experiment. The Gaussian beam imaging results were found to compare favorably with the ray/Born imaging results and provided somewhat smoother images.

Acknowledgements. This work was supported in part by the National Science Foundation and partly by the members of the Geo-Mathematical Imaging Group (GMIG) at Purdue University.

REFERENCES

[1] Aki, K. and P. Richards, (1980) *Quantitative Seismology*, Freeman, San Francisco.

[2] Bostock, M.G. and S. Rondenay, (1999) *Migration of scattered teleseismic body waves*, Geophys. J. Int., 137, 732-746.

[3] Bostock, M.G., S. Rondenay, and J. Shragge, (2001) *Multiparameter two-dimensional inversion of scattered teleseismic body waves 1. Theory for oblique incidence*, J. Geophys. Res., 106, 30,771-30,782.

[4] Bostock, M.G. (2004) *Green's functions, source signatures, and the normalization of teleseismic wavefields*, J. Geophys. Res., 109, B03303.

[5] Cerveny, V., (1985a) *Gaussian beam synthetic seismograms*, J. Geophys., 58, 44-72.

[6] Cerveny, V., (1985b) *The applications of ray tracing to the numerical modeling of seismic wave fields in complex structures*, in Seismic Shear Waves (ed. G. Dohr) Geophysical Press, London, pp. 1-124.

[7] Cerveny, V., (2000) *Seismic Ray Theory*, Cambridge University Press.

[8] Cerveny, V., M.M. Popov and I. Psencík, (1982) *Computation of wavefields in inhomogeneous media – Gaussian beam approach*, Geophys. J.R. Astr. Soc., 70, 109-128.

[9] Dasgupta, S. and R. L. Nowack, (2006) *Deconvolution of three-component teleseismic P-waves using the autocorrelation of the P to SV scattered waves*, Bull. Seism. Soc. Am., 96, 1827-1835.

[10] Dueker, K.G. and A.F. Sheehan, (1997) *Mantle Discontinuity structure from midpoint stacks of converted P to S waves across the Yellowstone hotspot track*, J. Geophys. Res., 102, 8313-8327.

[11] Hale, D., (1992) *Migration by the Kirchhoff, slant stack and Gaussian beam methods*, CWD-121, Center for Wave Phenomena, Colorado School of Mines, Golden, CO.

[12] Hill, N. R., (1990) *Gaussian beam migration*, Geophysics, 55, 1416-1428.

[13] Hill, N. R., (2001) *Prestack Gaussian beam depth migration*, Geophysics, 66, 1240-1250.

[14] Langston, C.A., (1977) *Corvallis, Oregon, crustal and upper mantle receiver structure from teleseismic P and S waves*, Bull. Seism. Soc. Am., 67, 713-724.

[15] Langston, C.A., (1979) *Structure under Mount Rainier, inferred from teleseismic body waves*, J. Geophys. Res, 84, 4749-4762.

[16] Nowack, R. L., (2003) *Calculation of synthetic seismograms with Gaussian Beams*, Pure and Applied Geophys., 160, 487-507.

[17] Nowack, R. L. and K. Aki, (1984) *The two-dimensional Gaussian beam synthetic method: testing and application*, J. Geophys., 89, 7797-7819.

[18] Nowack, R. L., W. P. Chen, U. Kruse and S. Dasgupta, (2007a) *Imaging offsets in the Moho: synthetic tests using Gaussian beams with teleseismic waves*, Pure and Applied Geophysics, 164, 1921-1936.

[19] Nowack, R. L., W. P. Chen, T.L. Tseng and the Hi-CLIMB Imaging Team, (2007b) *Imaging the crust and upper mantle beneath the Hi-CLIMB seismic array in Tibet using Gaussian beam migration of radial receiver functions*, Fall 2007 American Geophys. Union Meeting, San Francisco.

[20] Nowack, R. L., S. Dasgupta, G.T. Schuster and J.M. Sheng, (2006) *Correlation migration using Gaussian beams of scattered teleseismic body waves*, Bull. Seism. Soc. Am., 96, 1-10.

[21] Nowack, R. L., M.K. Sen and P.L. Stoffa, (2003) *Gaussian beam migration for sparse common-shot and common-reciever data*, SEG Int. Exposition and Seventy Third Annual Meeting, 1114-1117.

[22] Owens, T.J., G. Zandt and S.R. Taylor, (1984) *Seismic evidence from an ancient rift beneath the Cumberland Plateau, Tennessee: A detailed analysis of broadband teleseismic P waveforms*, J. Geophys. Res., 89, 7783-7795.

[23] Pavlis, G. L., (2003) *Imaging the earth with passive seismic arrays*, the Leading Edge, March, 224-231.

[24] Popov, M.M., (1982) *A new method of computation of wave fields using Gaussian beams*, Wave Motion, 4, 85-97.

[25] Poppeliers, C. and G.L. Pavlis, (2002) *Three-dimensional, prestack, plane wave migration of teleseismic P-to-S converted phases: 1. Theory*, J. Geophys. Res., 108, art. no. 2112.

[26] Rickett, J. and J. Claerbout, (1999) *Acoustic daylight imaging via spectral factorization: helioseismology and reservoir monitoring*, Leading Edge, 957-960.

[27] Rondenay, S., M.G. Bostock and J. Shragge, (2001) *Multiparameter two-dimensional inversion of scattered teleseismic waves 3. Application to the Cascadia 1993 data set*, J. Geophys. Res., 106, 30,795-30,807.

[28] Ryberg, T. and M. Weber, (2000) *Receiver function arrays: a reflection seismic approach*, Geophys. J. Int., 141, 1-11.

[29] Schuster, G. T., (2008) *Seismic Interferometry*, Cambridge Univ. Press, in press.

[30] Schuster, G.T., F. Followill, F. Katz, J. Yu and Z. Liu, (2003) *Autocorrelation migration: Theory*, Geophysics, 68, 1685-1694.

[31] Schuster, G.T., J. Yu, J. Sheng and J. Rickett, (2004) *Interferometric/daylight seismic imaging*, Geophys. J. Int. 157, 838-852.

[32] Sheehan, A.F., P.M. Shearer, H.J. Gilbert and K.G. Dueker, (2000) *Seismic Migration processing of P-SV converted phases for mantle discontinuity structure beneath the Snake River Plain, Western United States*, J. Geophys. Res., 105, 19,055-19,065.

[33] Sheng, J., G.T. Schuster and R.L. Nowack, (2001) *Imaging of crustal layers by teleseismic ghosts*, Trans. Am. Geophys. Un., EOS, Vol. 82.

[34] Sheng, J. G.T. Schuster, J.C. Pechman, K.L, Pankow and R.L. Nowack, (2003) *Coherence-weighted*

wavepath migration for teleseismic waves, Trans. Am. Geophys. Un. (EOS), Vol. 84, p. F5991.

[35] Shragge, J., M.G. Bostock and S. Rondenay, (2001) *Multidimensional inversion of scattered teleseismic body waves 2. Numerical examples*, J. Geophys. Res., 106, 30783-30793.

[36] Vinnik, L.P., (1977) *Detection of waves converted from P to PV in the mantle*, Phys. Earth planet. Inter., 15, 39-45.

[37] Yu, J., L.J. Katz, F. Followill, H. Sun and G.T. Schuster, (2003) *Autocorrelation migration: IVSPWD test*, Geophysics, 68, 297-307.

[38] Zhu, L., (2000) *Crustal structure across the San Andreas Fault, Southern California from teleseismic converted waves*, Earth Planet. Sci. Lett., 179, 183-190.